3-16-2010

Normal and Reverse Faulting Driven by the Subduction Zone Earthquake Cycle in the Northern Chilean Forearc

John P. Loveless
Smith College, jloveles@smith.edu

Richard W. Allmendinger
Cornell University

Matthew E. Pritchard
Cornell University

Gabriel González
Universidad Católica del Norte,

Normal and reverse faulting driven by the subduction zone earthquake cycle in the northern Chilean fore arc

John P. Loveless,[1,2] Richard W. Allmendinger,[1] Matthew E. Pritchard,[1] and Gabriel González[3]

Received 12 February 2009; revised 29 July 2009; accepted 5 October 2009; published 16 March 2010.

[1] Despite its location in a convergent tectonic setting, the Coastal Cordillera of northern Chile between 21°S and 25°S is dominated by structures demonstrating extension in the direction of plate convergence. In some locations, however, normal faults have been reactivated as reverse faults, complicating the interpretation of long-term strain. In order to place these new observations in a tectonic context, we model stress changes induced on these faults by the subduction earthquake cycle. Our simulations predict that interseismic locking on the plate boundary encourages normal slip on fore-arc faults, which may result from elastic rebound due to interplate earthquakes or from seismic or aseismic motion that takes place within the interseismic period. Conversely, stress generated by strong subduction zone earthquakes, such as the 1995 M_w = 8.1 Antofagasta event, provides a mechanism for the reverse reactivation we document here. Upper plate fault slip in response to the low-magnitude stress changes induced by the subduction earthquake cycle suggests that the absolute level of stress on these faults is very low. Furthermore, seismic hazard analysis for northern Chile requires consideration of not only the plate boundary earthquake cycle but also the cycle on fore-arc faults that may or may not coincide with the interplate pattern. Though the relationships between permanent strain and deformation calculated using elastic models remain unclear, the compatibility of modeled stress fields with the distribution of fore-arc faulting suggests that interseismic strain accumulation and coseismic deformation on the subduction megathrust both play significant roles in shaping structural behavior in the upper plate. **Citation:** Loveless, J. P., R. W. Allmendinger, M. E. Pritchard, and G. González (2010), Normal and reverse faulting driven by the subduction zone earthquake cycle in the northern Chilean fore arc, *Tectonics*, *29*, TC2001, doi:10.1029/2009TC002465.

1. Introduction

[2] Neogene deformation in the northern Chilean fore arc (21–25°S) above the interplate seismogenic zone is dominated by structures indicating extension in the direction of plate convergence. Numerous normal faults and open cracks striking approximately north-south occur both onshore and offshore [*Arabasz*, 1971; *Delouis et al.*, 1998; *González et al.*, 2003; *von Huene and Ranero*, 2003; *Loveless et al.*, 2005]. Several hypotheses have been put forth to explain the observed extension within a tectonic setting otherwise characterized by shortening, including (1) extension and uplift associated with subduction erosion [*Armijo and Thiele*, 1990; *Niemeyer et al.*, 1996; *Delouis et al.*, 1998; *von Huene et al.*, 1999; *Sallarés and Ranero*, 2005]; (2) coseismic release of strain accumulated during interseismic periods [*Delouis et al.*, 1998; *Loveless et al.*, 2005]; and (3) strains associated with the interseismic locking on the plate boundary, possibly related to flexural effects [*Delouis et al.*, 1998; *González et al.*, 2003; *Loveless et al.*, 2005]. These potential sources of stress likely act in concert to drive the observed margin-normal extension in the fore arc, with the long-term, static stress field caused by subduction erosion modulated by shorter-term earthquake cycle-related stresses.

[3] In some localities in the northern Chilean fore arc, we document reverse motion superimposed on the normal faulting scarp, which in at least one case reflects the most recent episode of fault slip. Such a pattern of reversal of the long-term slip sense has also been noted in other tectonic settings. Slip on faults in the Eastern California Shear Zone triggered by the 1999 Hector Mine earthquake was left-lateral, although the cumulative sense of geologic offset on these structures is right-lateral [*Fialko et al.*, 2002]. The reversal in strike-slip sense is attributed to localized stress changes induced by the earthquake within very weak fault zones. In past two decades, reverse slip has been noted on normal faults in the actively extending [*Puskas et al.*, 2007] Yellowstone-Teton region [*Hampel and Hetzel*, 2008]. In this case, the reversal of dip-slip motion is interpreted to be driven by the inflating and deflating Yellowstone magma chamber. These examples illustrate two characteristics allowing cyclic behavior of faults: anomalous (weak) material properties within fault zones and perturbations to the stress field loading the faults. We extend these concepts

[1]Department of Earth and Atmospheric Sciences, Cornell University, Ithaca, New York, USA.
[2]Now at Department of Earth and Planetary Sciences, Harvard University, Cambridge, Massachusetts, USA.
[3]Departmento de Ciencias Geológicas, Universidad Católica del Norte, Antofagasta, Chile.

0278-7407/10/2009TC002465

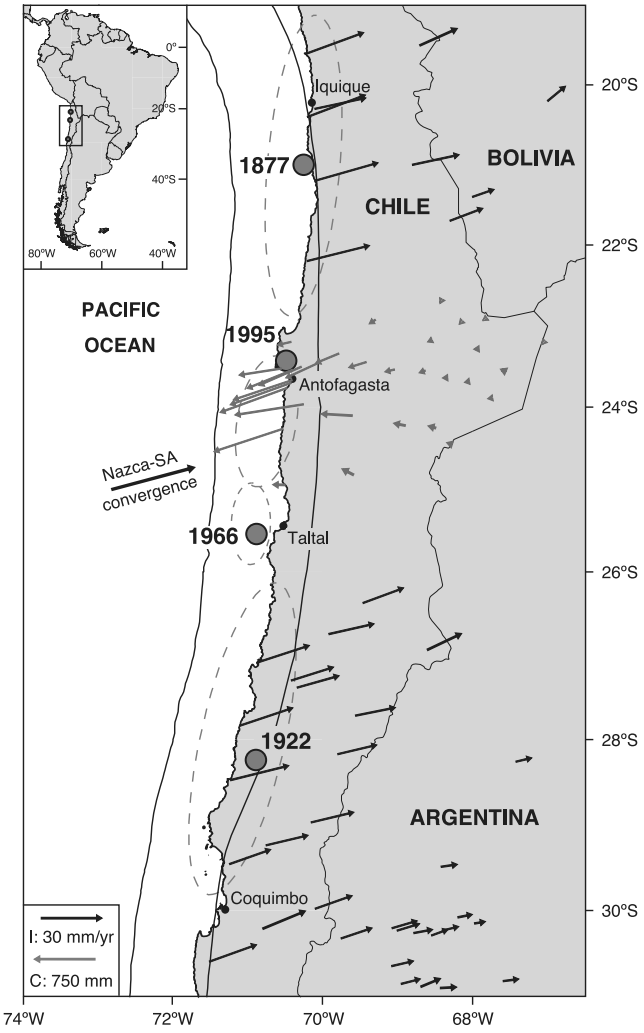

Figure 1. Seismotectonic setting of the northern Chilean fore arc. Interseismic shortening on the scale of the orogen is demonstrated by the eastward decrease in GPS velocity (black vectors, length scale labeled "I"), while elastic rebound during the 1995 Antofagasta earthquake is shown by the westward increase in coseismic GPS displacement (gray arrows, length scale labeled "C"). Interseismic data north of Antofagasta are from *Kendrick et al.* [2001] and from *Brooks et al.* [2003] to the south. Interseismic data are contaminated by the coseismic and postseismic signal of the 1995 earthquake. Coseismic data are from *Klotz et al.* [1999]. Nazca–South America convergence vector shows approximate direction but not magnitude of relative plate motion. Dashed ovals show approximate rupture areas of several prominent underthrusting earthquakes; circles mark the actual or inferred epicenters (data from *Kelleher* [1972], *Comte and Pardo* [1991], and *Ruegg et al.* [1996]). The solid black lines show the surface projection of the trench and 50 km slab contour [*Cahill and Isacks*, 1992].

to northern Chile, suggesting in this paper that (1) fore-arc faults have sustained damage through fault slip throughout their long (Mesozoic–recent) history and thus are likely very weak and (2) natural variations in the stress applied to them result from the subduction zone earthquake cycle.

[4] We use models of stress changes induced by the subduction zone earthquake cycle to investigate the relationships between upper plate fault motion and the underlying plate boundary processes, placing our new field observations in the context of the large-scale tectonics. We calculate the near-surface stress field generated by interseismic locking and coseismic slip on the subduction zone using elastic dislocation models, investigating the effects of variation in locking depth of the subduction interface. We focus on the region near the city of Antofagasta (23.5°S), where numerous well-developed fault scarps and some exposed fault planes provide information about the kinematics of permanent deformation [*Delouis et al.*, 1998; *González et al.*, 2003; *Allmendinger and González*, 2010]. The seismic cycle and permanent surface deformation are fundamentally driven by the same processes [*Allmendinger et al.*, 2005, 2007], which implies their interdependence. Numerous previous studies in the Andean fore arc have used elastic modeling of geodetic data to extract information about subduction processes [e.g., *Klotz et al.*, 1999; *Bevis et al.*, 2001; *Pritchard et al.*, 2002; *Khazaradze and Klotz*, 2003; *Pritchard et al.*, 2006], and we suggest here that geological data also offer insight into the properties of the plate boundary interface. Unlike the geodetic measurements, which record only a snapshot of the tectonics, the permanent deformation fields reflect plate boundary strain accumulated over many earthquake cycles. Furthermore, our assessment of upper plate faults provides insight into their seismogenic potential, as a full evaluation of seismic hazard in the northern Chilean fore arc requires consideration not only of the subduction megathrust, but also earthquakes that may occur in the upper plate.

2. Tectonic and Geological Setting

[5] For the past 25 Myr, convergence across the strongly coupled interface between the Nazca and South American plates has resulted in significant crustal thickening and shortening. Presently, relative plate motion is locally described by a vector with velocity ~65 mm/yr directed ~075° along the northern Chilean coastline (Figure 1) [*Kendrick et al.*, 2001]. Elastic dislocation modeling of interseismic GPS data suggests that, during the interseismic period, the plate interface is coupled between depths of 20 and 35–50 km [*Bevis et al.*, 2001; *Khazaradze and Klotz*, 2003], which is broadly consistent with the extent of the seismogenic zone as determined by inversion of teleseismic waveforms [*Tichelaar and Ruff*, 1991]. GPS data capture shortening in the direction of plate convergence on the scale of the orogen during the interseismic period [*Kendrick et al.*, 2001; *Bevis et al.*, 2001; *Brooks et al.*, 2003; *Chlieh et al.*, 2004] and extension of the fore arc in the same direction during subduction earthquakes (Figure 1) [*Ruegg et al.*, 1996; *Klotz et al.*, 1999]. Much of the strain that accumu-

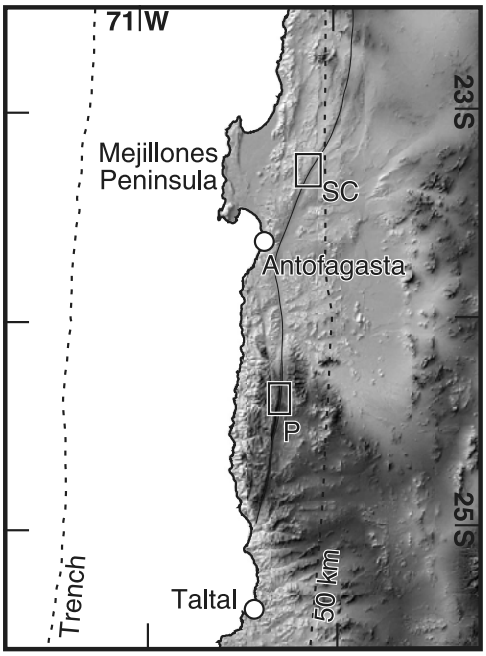

Figure 2. Shaded relief topography map showing key localities in the Antofagasta region. Black dashed lines show surface projections of subduction trench and 50 km Wadati-Benioff zone contour [*Cahill and Isacks*, 1992]. Thin black line marks the trace of the Atacama Fault System (AFS) and other prominent topographic scarps mark subsidiary faults. SC, Salar del Carmen segment of the AFS (section 3.1); P, Paposo segment (section 3.2).

lates in the upper plate due to the locked plate boundary during the interseismic period is relieved by strong subduction earthquakes, the recurrence interval of which is estimated to be 100–150 years in northern Chile [*Comte and Pardo*, 1991].

[6] The Coastal Cordillera of the northern Chile fore arc represents a relic of the Mesozoic Andean arc and comprises dominantly Late Jurassic and Cretaceous plutonic and volcanic rocks. Bedrock exposure is generally poor as the surface is blanketed with gypsum-indurated regolith ("gypcrete" [*Rech et al.*, 2003, 2006]). The hyperarid climate of the Atacama Desert, which has persisted since the Miocene (6 Ma [*Hartley and Chong*, 2002] and 23–13 Ma [*Dunai et al.*, 2005; *Rech et al.*, 2006]), allows for long-term preservation of surface features. The principal structure of the northern Chilean fore arc is the Atacama Fault System (AFS, black lines in Figure 2), which originated in the Mesozoic as a major strike-slip structure [*Arabasz*, 1971; *Naranjo*, 1987; *Scheuber and Andriessen*, 1990; *Scheuber and González*, 1999; *Delouis et al.*, 1998; *González et al.*, 2003]. Major faults of the Coastal Cordillera have strongly deformed the country rocks. We note that faults are characterized by a weak core comprising 1–3 m of gouge surrounded by at least 100 m of cataclastic rocks. Damage zones extend laterally several hundred meters from the fault trace.

2.1. Neotectonics of the Antofagasta Region

[7] Whereas numerous margin-parallel faults in the Coastal Cordillera are of suspected Mesozoic strike-slip origin, field studies indicate that they have experienced primarily dip-slip neotectonic reactivation [*Arabasz*, 1971; *Armijo and Thiele*, 1990; *Delouis et al.*, 1998; *Riquelme et al.*, 2003; *González et al.*, 2003, 2006; *Allmendinger and González*, 2010]. Compilations of fault kinematic data from the Mejillones Peninsula and the Salar del Carmen segment of the AFS (Figure 2) show fault plane solutions consistent with normal faulting due to east-west extension [*Delouis et al.*, 1998; *González et al.*, 2003]. Dextral slip indicators on northwest striking faults in the Salar Grande region (21°S [*González et al.*, 2003; *Carrizo et al.*, 2008]) and the Barazarte fault southeast of Antofagasta [*Delouis et al.*, 1998] are kinematically consistent with regional east-west extension. The activity level and slip recurrence interval of faults are poorly constrained, primarily due to the lack of dateable organic material within faulted sediments. *González et al.* [2006] present cosmogenic dating of alluvial fan surfaces that constrains motion on the Salar del Carmen segment of the AFS to be younger than 424 ± 151 ka, while *Carrizo et al.* [2008] suggest post-300 ka faulting in the Salar Grande region on the basis of an offset tuff. Scarp morphology dating suggests scarp ages ranging between 16 and 400 ka; the large range reflects uncertainty, stemming from the hyperarid climate, in the diffusion constant used in the dating [*González and Carrizo*, 2003]. The hyperaridity of the region is capable of preserving structures for long periods of time; ruptures with a fresh appearance may reflect deformation that occurred thousands of years ago [*González and Carrizo*, 2003; *González et al.*, 2006]. Recent reactivation of faults is suggested by vertical offset of 15–20 cm along the Paposo segment of the AFS, located south of Antofagasta around 25°S latitude [*Delouis et al.*, 1997, 1998; *Klotz et al.*, 1999], and along the Salar del Carmen segment [*Klotz et al.*, 1999], which were reported to have accompanied the 1995 M_w = 8.1 subduction zone earthquake, which occurred offshore Antofagasta.

3. New Structural Observations

[8] New field observations at several key localities in the Antofagasta region augment the neotectonic database described above. Along the northern part of the Salar del Carmen segment of the AFS (labeled "SC" on Figure 2), we observe evidence of minor reverse motion superimposed on a normal fault scarp. At a site along the Paposo segment of the AFS ("P" on Figure 2), we see morphological characteristics similar to those present at the Salar del Carmen site and thus infer the same style of fault reactivation.

3.1. Northern Salar del Carmen Segment of the AFS

[9] About 65 km northeast of Antofagasta at the northern end of the Salar del Carmen segment of the AFS (23.15°S, 70.06°W), we observe structural and morphological characteristics indicating that the basin at the foot of the scarp

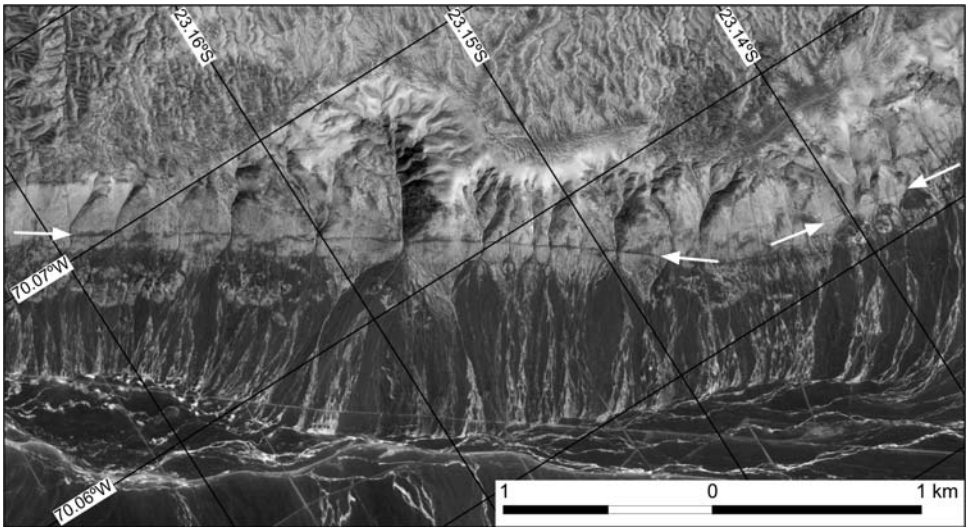

Figure 3. QuickBird satellite image of the site of reverse fault reactivation of the northern Salar del Carmen segment of the Atacama Fault System. Locality is shown as box labeled "SC" in Figure 2. The topographic bench is highlighted by the arrows.

has moved up relative to the fault-bounded mountain front. In map view (Figure 3), the smooth, SE facing topographic scarp, which we interpret to have been constructed by normal slip on a SE dipping fault, features a narrow yet prominent dark band midway up the slope. The band marks a subtle topographic bench up to ~2 m wide on the scarp, where a gentler slope has allowed for accumulation of dark, coarse alluvium. Channels incising the scarp provide structural and morphological evidence for reverse fault motion along the Salar del Carmen scarp. Channels that are sufficiently deeply incised expose a wedge of basement rock in the hanging wall that is upthrust against the gypcrete cap of the footwall along a splay fault (Figure 4a). The magnitude of slip is estimated to be on the order of 1–2 m based on an irregularly exposed marker horizon. Uplift of the hanging wall has resulted in folding of gypsum indurated sediment (Figure 4a, inset) immediately above it, producing the topographic bench and broad warping of the modern surface of the hanging wall block, including the marker horizon. The uplift of the hanging wall relative to the footwall is further indicated by the change in incision style of scarp-perpendicular channels that occurs at the level of the reverse faulting. Above this height, channels show a smoother morphology, whereas below the topographic bench, incision into the hanging wall is more pronounced (Figure 4b), suggesting that the most recent episode of reverse faulting occurred prior to the latest fluvial downcutting. It is possible that the fault zone serves as a conduit for fluid flow, which could also contribute to the change in incision style at the level of the fault. Other anomalies in the scarp topography, as can be seen above the main topographic bench in Figure 4b, may represent minor amounts of normal or reverse faulting on other fault splays, or they may represent slumping of alluvium unrelated to faulting.

[10] The spatial correlation between the reverse faulting and the topographic bench allows the bench to be used as an indicator of the along-strike extent of reverse fault reactivation. Along the Salar del Carmen segment, the bench extends for about 2 km (Figure 3). The width of the bench as defined by the extent of anomalously dark surface cobble accumulation (Figure 3) is a function of the degree of surface curvature: the bench is narrower where the surface is more abruptly curved by the reverse faulting beneath and wider where the bench is more subtle. Given the relationships between the subsurface faulting and development of the topographic bench, as seen within and above the most deeply incised channels, the topographic bench width and curvature depends on the burial depth of the reverse fault and the amount of offset on it. A narrow, more abrupt bench correlates with a shallowly buried fault and/or greater slip, whereas the wider, subtler bench indicates a more deeply buried fault and/or less slip.

[11] Several details of the reverse faulting revealed in the canyon exposures lead to our preferred interpretation in Figure 5. Normal motion on the master thrust, along with degradation of the resulting scarp, have produced the dominant topography observed today (Figure 5a). In response to fault-normal compression, reverse motion occurs on a footwall cutoff (Figure 5b). The gypcrete regolith cap that blankets the entire fault scarp surface is distinctly warped by the upthrust basement wedge (Figures 4a and 5b). The lithologic relationships seen in the channel beds reveal the relationship between the fault responsible for the upthrusting of the basement wedge with the primary normal fault that has constructed the overall scarp. The composition of the channel bed changes, from gravel downstream of the topographic bench, to bedrock at the level of the bench, to gypsum-indurated gravel immediately upstream of the bench, and back to bedrock farther upstream (Figure 5b). The contact between the downstream bedrock and the intervening regolith coincides with the location of the reverse fault and topographic bench. The

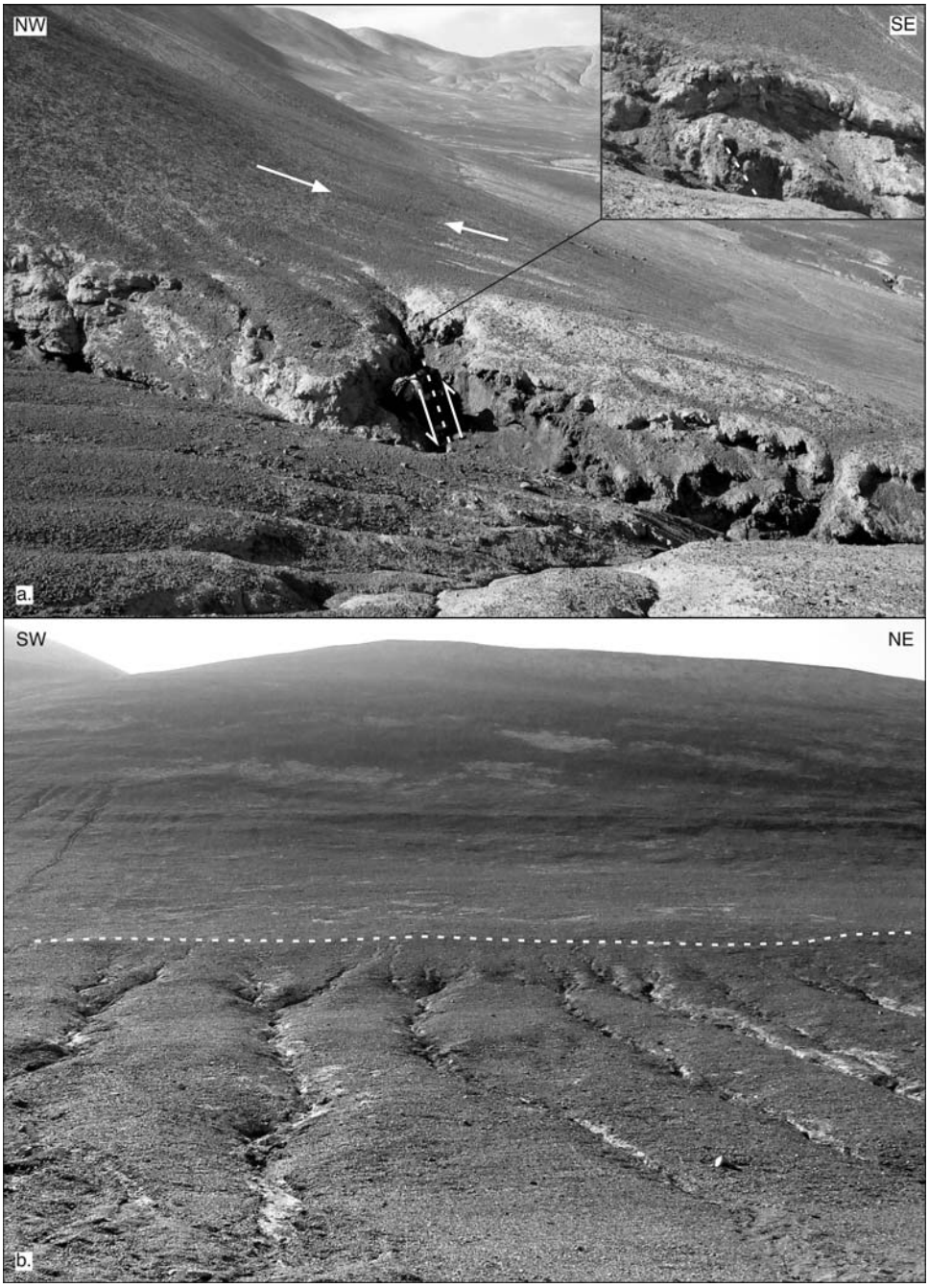

Figure 4. (a) Field photo showing exposure of reverse faulting in a scarp-perpendicular channel with topographic bench overlying the fault. White arrows on the scarp surface mark the topographic bench on which darker cobbles have accumulated. Dashed white line and half arrows show approximate location of fault and sense of motion. Geologist is for scale. Zoom photo demonstrates gypcrete folded by the reverse faulting. Dashed white line represents the approximate axial plane of the fault-related fold. (b) Field photo, taken facing scarp, showing the change in incision style coincident with the topographic bench (marked by white dashed line), from shallowly incised above the bench to more sharp below the bench.

contact between the regolith and the upstream bedrock is not marked by a change in the topography and represents a stratigraphic contact. These lithologic relationships suggest that the reverse faulting takes place on a footwall cutoff. It is also possible that the reverse fault splay is contained within the hanging wall block of the normal fault, but this geometry seems less likely than the fault located within the footwall, as the observed intervening stretch of channel bed composed of sediment is shorter than the width expected for this geometry.

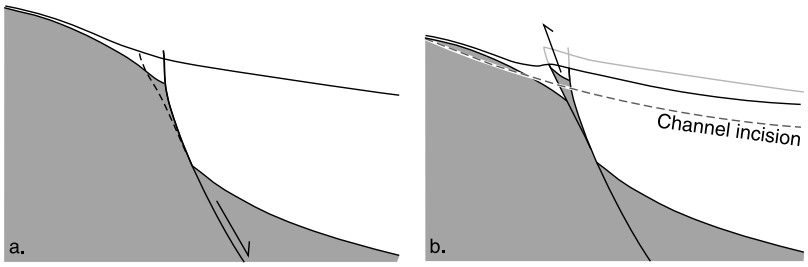

Figure 5. Conceptual model (not to scale) of reverse fault reactivation, as seen at the northern end of the Salar del Carmen fault. (a) Normal slip on the fault creates the initial fault scarp, which subsequently degrades into the modern smooth landform. (b) When subject to fault-normal compression, a footwall cutoff (dashed line in Figure 5a) experiences reverse motion, creating the subtle topographic bench observed at the surface and the upthrust basement wedge exposed in the drainages that crosscut the scarp. On the basis of the lithologic relationships observed in channels that incise the scarp (gray dashed line with white outline), a splay fault in the footwall or the hanging wall of the master normal fault are both plausible. The channel bed composition changes from sediment in the hanging wall, to bedrock near the level of the reverse fault, back to sediment above the fault, and finally back to bedrock farther upstream.

[12] In some of the crosscutting channels, no bedrock wedge is exposed at the level of the topographic bench. Instead, the composition of the channel bed changes from uniformly sediment downstream of the bench to bedrock upstream. The fact that bedrock is not exposed within the channel at the level of the bench suggests that (1) reverse motion has been limited, such that only the gypsum-indurated regolith is uplifted, (2) the location of reverse faulting is buried more deeply than in other canyons, or (3) reverse motion is taking place on a different fault splay, which may be located such that it uplifts a portion of the colluvial wedge constructed by primary normal faulting, rather than a slice of bedrock.

3.2. Northern Paposo Segment of the AFS

[13] Topographic characteristics similar to those seen at the northern Salar del Carmen segment site are observed along a 3.5 km long stretch of the scarp of the Paposo segment of the AFS (70 km south of Antofagasta; 24.32°S, 70.31°S). In this case, a topographic bench on the scarp is highlighted by alluvial material lighter in color than that covering other parts of the slope (Figure 6a). No channels dissect the scarp sufficiently to expose bedrock, but some shallow drainages do show a change in incision style at the height of the topographic bench, similar to those at the Salar del Carmen site. This change in channel morphology, from gently incised above the bench to more sharply incised below, in conjunction with the relative uplift of the hanging wall alluvial fan as seen in profile (Figure 6b), indicates about 1 m of reverse fault reactivation. About 70 km along strike to the south (at 24.94°S, 70.43°W), an exposure of the master normal fault in a pronounced canyon indicates a steep east dip. Such an orientation is consistent with that implied by the morphology of the cumulative normal fault scarp and suggestive of east-side-up reverse reactivation as the cause of the relative uplift of the alluvial fan surface.

[14] The cumulative reverse faulting (1–2 m) is far less than the total normal motion that has constructed the Salar del Carmen and Paposo scarps, indicating that normal motion is still the dominant mode of faulting in this region. That the reverse faulting takes place on a structure other than the principal normal fault may permit the topographic bench to continue to grow with each episode of reverse motion, rather than being "erased" by a subsequent instance of normal faulting. After many normal and reverse faulting events, a ridge-trench-ridge morphology would develop, with the upslope portion of the original normal fault scarp forming a ridge, separated from a smaller hanging wall ridge caused by reverse faulting-related warping by an intervening trench. Such a morphology is observed north of the Antofagasta region near Salar Grande [*Carrizo et al.*, 2008] and may indicate the future form of Antofagasta area faults.

4. Modeling Seismic Cycle Deformation

[15] The new field observations demonstrate complexity in the permanent strain field of the fore arc. Whereas previous studies of the neotectonics of the Antofagasta region have found fault kinematic indicators consistent with east-west extension [*Armijo and Thiele*, 1990; *Niemeyer et al.*, 1996; *Delouis et al.*, 1998; *González et al.*, 2003], the northern Salar del Carmen and Paposo faults also show signals of deformation indicative of east-west shortening. We use elastic dislocation models [e.g., *Savage*, 1983; *Okada*, 1985, 1992] to calculate the stress fields induced during the interseismic and coseismic periods of the subduction zone earthquake cycle and evaluate their compatibility with the observed structural styles.

4.1. Interseismic Modeling

[16] Over the course of an idealized, full seismic cycle (interseismic plus coseismic), relative motion between the subducting slab and overriding continent is characterized by thrust sense block motion. On the seismogenic portion of the plate interface, which is locked during the interseismic

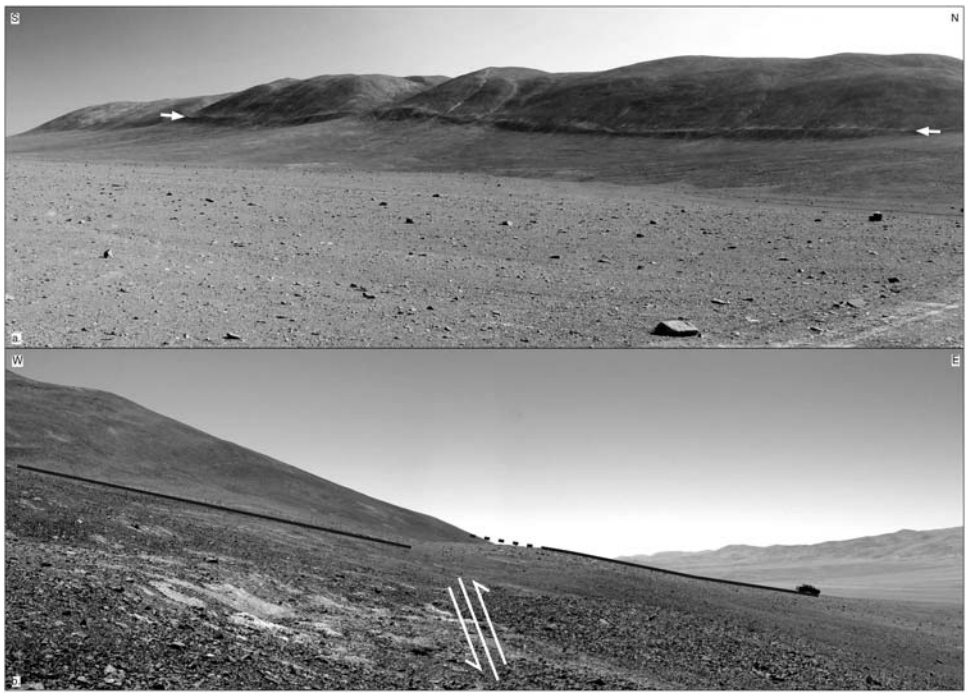

Figure 6. Site of inferred reverse fault reactivation of the northern Paposo segment of the Atacama Fault System. Locality is shown as a diamond along the fault labeled "P" in Figure 2. (a) Field photo looking obliquely at the scarp. The white arrows highlight the topographic bench, which is marked by an accumulation of alluvium lighter in color than that covering other parts of the slope. (b) Profile view of the scarp indicating the uplift of the hanging wall alluvial fan relative to the footwall. Offset is on the order of 1–2 m.

phase, this motion occurs during an earthquake. Elsewhere, thrust sense motion takes place as stable sliding throughout the interseismic period, which does not induce substantial stress change or strain accumulation in the upper plate. To model the strain accumulation that results from interseismic locking, we use a kinematic coseismic slip deficit model (e.g., the "back slip" convention of *Savage* [1983]). In this construction, interseismic strain accumulation in the upper plate is simulated by applying slip on the subduction interface that is equal and opposite to that expected to occur during an earthquake. Therefore, to the regions that are fully coupled during the interseismic period, which roughly coincide with the seismogenic zone, we apply normal sense slip at the plate convergence rate. In regions that are partially coupled, we apply slip deficit at a rate less than that of plate convergence. Summing this slip deficit with the long-term, thrust sense relative plate motion yields a kinematic representation of interseismic deformation, with no relative motion on the portion of the interface that is locked during the interseismic period and thrust sense motion where the slab and upper plate slide stably past each other.

4.1.1. Model Parameters

[17] We model the effects of interseismic strain accumulation due to slip deficit on the plate boundary interface using Poly3D, a three-dimensional boundary element program [*Thomas*, 1993]. This program calculates displacement, strain, and stress in a homogenous elastic half-space resulting from slip applied to a series of dislocations. We discretize the plate boundary into triangular dislocation elements, allowing the along-strike and downdip curvature of the interface to be accurately modeled. We use the method of *Wang et al.* [2003] to calculate magnitude and rake of slip deficit by projecting the Euler pole of relative plate motion as defined by *Kendrick et al.* [2001] onto each element. Because the modeling is carried out in an elastic half-space, we adjust the plate boundary geometry for topography and bathymetry [*Flück et al.*, 1997]. The plate boundary is divided into three regions: the partially coupled seaward transition zone, which extends from the trench to approximately 20 km depth; the fully locked portion of the interface, between 20 and 32–45 km depth; and the downdip, partially coupled transition zone, which extends 15 km deeper than the bottom of the locked zone (Figure 7). We discuss the implications of this zonation in section 6.1.

4.1.2. Slip Distribution

[18] We apply slip deficit at the plate convergence rate to the locked portion of the subduction fault in order to model interseismic strain accumulation. Within the transition zones, the applied back slip magnitude lies between zero and the convergence rate. In general, with increasing depth, subducted material lying at the plate interface within updip (seaward) transition zone is progressively dewatered, allowing for the transition from stable to unstable interplate sliding [*Oleskevich et al.*, 1999]. Downdip of the locked zone, the interface behavior experiences a transition from stick-slip to thermally activated stable sliding [*Oleskevich et*

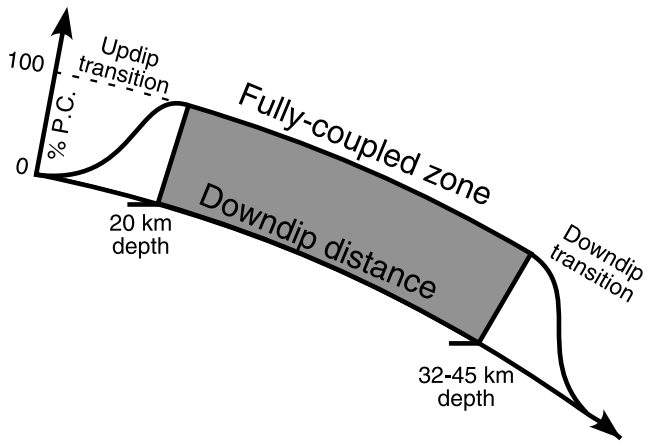

Figure 7. Schematic slip deficit distribution on the subduction zone interface. We use a Gaussian function (equation (1)) to smoothly taper the slip deficit magnitude from its maximum value equal to the plate convergence rate, representing full coupling, to zero within the partially coupled transition zones.

al., 1999]. Smoothly tapering the slip within the transition zones serves as a kinematic approximation for the presumably gradual changes in physical behavior [e.g., *Wang et al.*, 2003; *Chlieh et al.*, 2004]. We use a Gaussian function, shown schematically in Figure 7, that minimizes abrupt changes in slip magnitude which could produce concentrations of near-surface strain [e.g., *Savage*, 1983]. The slip magnitude, u', on each element within the transition zones is described as

$$u' = u \exp\left(\frac{-s^2}{2c^2}\right) \quad (1)$$

where u is the slip magnitude of the fully locked element nearest the particular transition zone element, s is the downdip position of the transition zone element relative to the extent of that zone, and c is a shape factor governing the curvature of the slip transition.

[19] The maximum depth of interplate locking has been addressed by several studies in northern Chile [*Tichelaar and Ruff*, 1991; *Comte et al.*, 1994; *Delouis et al.*, 1996; *Bevis et al.*, 2001; *Khazaradze and Klotz*, 2003; *Chlieh et al.*, 2004]. Ambiguity in the definition of the term "plate coupling" has been discussed previously [*Wang and Dixon*, 2004a] and we here present the concepts relevant to our models. Variation in the nature of the interface between the subducting and overriding plates in a subduction zone can be characterized using frictional or kinematic boundary conditions. The frictional conditions on the interface vary from those that allow stable sliding to those consistent with unstable or stick-slip interaction [e.g., *Pacheco et al.*, 1993]. Kinematic boundary conditions describe relative motion between the plates ranging from slipping at the rate of plate convergence to not slipping. Equivalence between the frictional and kinematic descriptions of interplate behavior is not clearly established [*Wang et al.*, 2003; *Wang and Dixon*, 2004a; *Lay and Schwartz*, 2004; *Wang and Dixon*, 2004b]. We note that the 20–50 km depth extent of kinematic locking (i.e., no relative motion) inferred from surface GPS velocities [*Bevis et al.*, 2001] agrees with the observed depth range of underthrusting earthquakes [*Tichelaar and Ruff*, 1991], indicating that, to a first order, the zone of kinematic interplate locking and the seismogenic zone coincide. In our modeling of the seismic cycle, we use information regarding the extent of locking used to model GPS data [e.g., *Bevis et al.*, 2001; *Khazaradze and Klotz*, 2003] as well as the depth range of the seismogenic zone [e.g., *Tichelaar and Ruff*, 1991; *Comte et al.*, 1994; *Delouis et al.*, 1996].

[20] *Tichelaar and Ruff* [1991] used seismic waveform inversion to deduce that the maximum seismogenic depth is at least 45–48 km for northern Chile (18°–24°S), no deeper than 36–41 km for the Taltal region (24°–27°S), and at least 48–53 km in the Copiapó region (27°–30°S). Thus, transitions between deeper and shallower coupling take place around the latitudes of Antofagasta and Copiapó. In their local seismic study of the Antofagasta region, *Delouis et al.* [1996] noted a "reduced" number of earthquakes occurring between 35 and 50 km depth and indicate that these events are more consistent with reverse faulting than underthrusting. *Khazaradze and Klotz* [2003] showed a change in extent of coupling from 50 km to 35 km depth around the latitude of the Mejillones Peninsula based on elastic modeling of GPS data, though their modeling is complicated in the region of the transition by postseismic deformation associated with the 1995 Antofagasta earthquake and the low density of stations from 25–30°S. *Comte et al.* [1994] suggested that the maximum depth of the coupled interplate zone is 47 km throughout the Antofagasta region based on locations of thrust-type earthquakes. By inverting geodetic and seismic data, *Pritchard et al.* [2006] determined the slip distributions for 11 $M_w > 6$ earthquakes in the Antofagasta region. The largest earthquake studied (the 1995 event) ruptured the plate boundary to a depth of ~40 km, while four smaller earthquakes occurred farther downdip. *Pritchard et al.* [2006] propose that the interface between 40 and 50 km depth may be characterized by discontinuous patches within which the smaller earthquakes can nucleate, but surrounded by stably sliding regions. The kinematic definition of the transition zone serves as a gross approximation for such heterogeneity: because only isolated portions of the interface slip seismically in a given earthquake, it is likely that interseismic strain accumulation occurs primarily on these patches, with lesser accumulated strain in the intervening, stably sliding regions.

[21] We model a change in the maximum depth of full interplate locking around the latitude of the Mejillones Peninsula (23.5°S), based the observations of the seismogenic zone described above. North of this latitude, the locked portion of the plate interface extends from 20 to 45 km, with transitional slip to 60 km. This extent of locking is consistent with the elastic modeling of interseismic GPS data in northern Chile and southern Peru [*Bevis et al.*, 2001; *Chlieh et al.*, 2004]. Near Antofagasta, we model

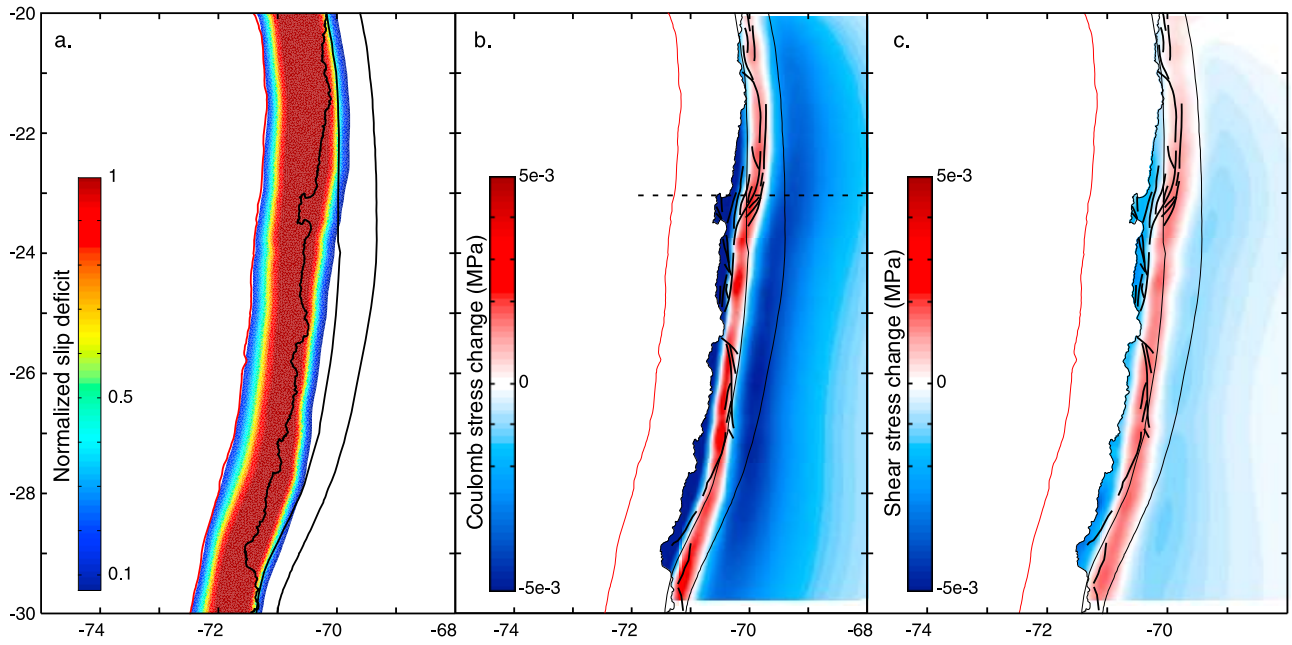

Figure 8. (a) Input slip deficit normalized by maximum magnitude. The slip values are calculated by projecting the Euler pole of relative plate convergence [*Kendrick et al.*, 2001] onto the triangular dislocation elements representing the plate boundary [*Wang et al.*, 2003]. The extent of full interplate coupling lies between 20 and 50 km depth in northernmost Chile and decreases to between 20 and 38 km around the latitude of the Mejillones Peninsula. Updip and downdip of this zone are transition zones within which the back slip magnitude decreases smoothly from the maximum value to zero. See section 4.1.2 for more details. (b) Coulomb stress change due to 1 year of interseismic locking, calculated using the slip distribution shown in Figure 8a. The Coulomb stress change is resolved on planes striking 010°, dipping 80°, with a slip vector of −110°, and is calculated at the surface assuming an effective coefficient of friction of $\mu' = 0.4$. Dashed horizontal line shows the position of the profile shown in Figure 10. (c) Shear stress change resolved on planes with same orientation and rake described in Figure 8a. In Figures 8a–8c, the red line offshore shows the position of the trench, while nearly parallel black lines onshore show the 50 km (west) and 75 km (east) contours of the Wadati-Benioff zone. Bold discontinuous lines in fore arc show prominent fault traces.

locking between 20 and 32 km, with transitional slip to 47 km. We follow the geometry described by *Tichelaar and Ruff* [1991] for the Copiapó region and smoothly increase the width of the coupled zone around 27°S (Figure 8a).

5. Modeling Results

[22] Models of interseismic loading in the Antofagasta region show patterns of deformation consistent with the distribution of normal faults. We use the calculated stress tensor to determine the Coulomb stress change ($\Delta\sigma_c$), which provides a single, convenient quantity used to evaluate how the subduction zone processes influence the upper plate structures. $\Delta\sigma_c$ is defined as

$$\Delta\sigma_c = \Delta\tau - \mu'\Delta\sigma_n, \tag{2}$$

where $\Delta\tau$ is the change in shear stress in a particular direction (rake), μ' is the effective coefficient of friction (accounting for pore fluid pressure), and $\Delta\sigma_n$ is the change in stress acting normal to the fault plane. All quantities represent conditions on fault planes of a specified orientation with a slip vector of specified rake. We calculate $\Delta\sigma_c$ resolved on planes striking 010° and dipping 75°E, with $\mu' = 0.4$ and a slip vector of rake −110° (i.e., normal fault slip). These values are broadly consistent with the fault geometries and kinematic indicators observed around Antofagasta [*Delouis et al.*, 1998; *González et al.*, 2003], and variation of any angular parameter by ±10° does not substantially affect the distribution of $\Delta\sigma_c$. Faults lying within zones of positive $\Delta\sigma_c$ are moved closer to failure by interseismic plate boundary locking, whereas normal faulting is discouraged on faults lying within regions of negative $\Delta\sigma_c$. The quantity $\Delta\sigma_c$ encompasses changes in shear and/or normal stresses on a fault plane, plus a possible change in the frictional coefficient. Thus, a negative $\Delta\sigma_c$ can indicate encouragement toward failure in a direction opposite the specified rake, i.e., reverse faulting according to our convention. We do not explicitly model a regional stress field. Rather, the distribution of $\Delta\sigma_c$ represents solely the effect of the seismic cycle on the state of stress on upper plate faults.

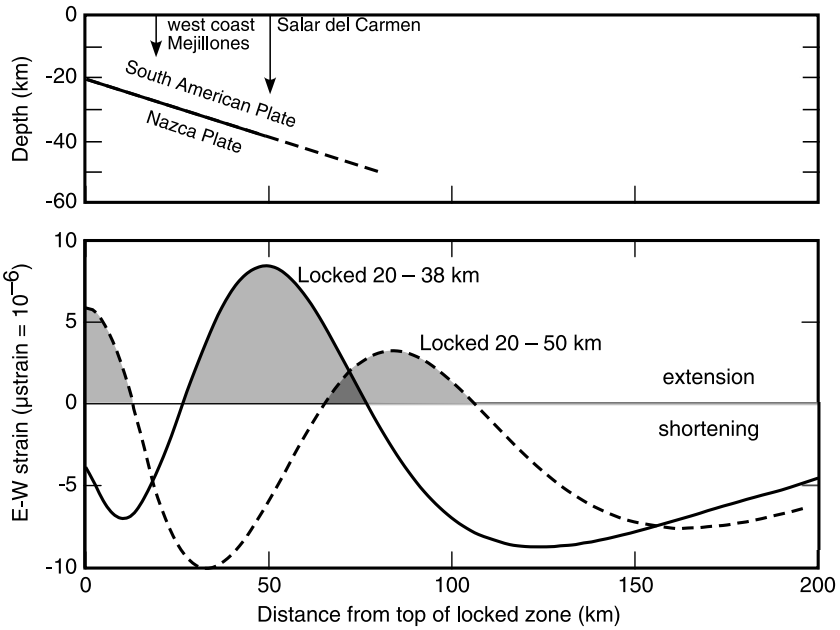

Figure 9. Comparison of the trench-perpendicular (east-west) surface strain field resulting from dipping dislocations with two different locking depths. The zone of extension resulting from interplate locking between 20 and 38 km depth is greater magnitude but narrower in longitudinal extent than that resulting from locking between 20 and 50 km depth.

Calculating $\Delta\sigma_c$ using the deviatoric rather than full stress tensor yields a very similar pattern, as does calculation using the alternate formula proposed by *Beeler et al.* [2000].

[23] Figure 8b shows the distribution of $\Delta\sigma_c$ at the surface resulting from 1 year of interseismic convergence. Positive $\Delta\sigma_c$ is predicted within a narrow region of the Coastal Cordillera and shows a spatial correlation with the downdip extent of the coupled plate interface (Figure 9). The change in locking depth we introduce around the Mejillones Peninsula results in a distribution of positive $\Delta\sigma_c$ that is consistent with the trace of the AFS along the Salar del Carmen segment (Figure 8b). The Paposo segment of the AFS lies on the edge of the region of positive $\Delta\sigma_c$, and some faults immediately west of it lie within the zone of negative $\Delta\sigma_c$. *Naranjo* [1987] suggested that these faults have been inactive since 10 Ma, but the reported normal faulting induced by the 1995 Antofagasta earthquake [*Delouis et al.*, 1997, 1998], as well as the reverse faulting we describe in section 3.2 suggest otherwise. The numerous examples of recent normal faulting on the Mejillones Peninsula show poor correlation with the pattern of interseismic $\Delta\sigma_c$; we address some potential explanations for this discrepancy in the discussion. The shear stress change $\Delta\tau$ is also positive within a narrow zone near the coastline (Figure 8c), demonstrating that interseismic convergence increases downdip shear stress on the normal fault planes. Stress change normal to the specified fault planes ($\Delta\sigma_n$, not shown) is distributed similarly to $\Delta\sigma_c$, which means that the AFS and nearby faults are unclamped due to convergence, likely as the result of flexure of the continental plate. Positive $\Delta\sigma_c$ is restricted to the near-surface region shallower than 2–3 km (Figure 10), suggesting that the traction free condition at the Earth's surface plays an important role in dictating the shallow stress field. The depth limitation of zone of positive $\Delta\sigma_c$ is consistent with the style of deformation that we observe, with short-wavelength fault-related topography suggesting depth of motion very near the surface.

5.1. Effects of Subduction Zone Earthquakes

[24] Using the 1995 M_w = 8.1 Antofagasta event as an example, *Loveless and Pritchard* [2008] show that fore-arc

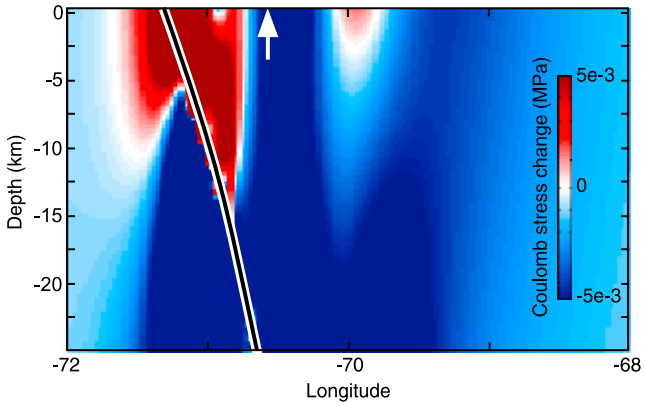

Figure 10. Profile view of 1 year of interseismic Coulomb stress change, calculating along the dashed line in Figure 8b. The white arrow shows the approximate position of the coastline. The onshore zone of positive Coulomb stress change is restricted to depths shallower than 2–3 km.

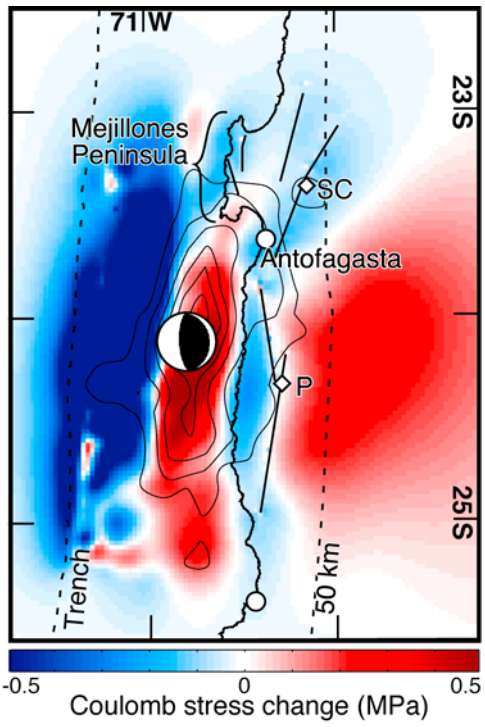

Figure 11. Preferred model of coseismic upper plate $\Delta\sigma_c$ induced by the 1995 M_w = 8.1 Antofagasta earthquake [*Loveless and Pritchard*, 2008]. $\Delta\sigma_c$ is calculated using the slip distribution of *Pritchard et al.* [2006] and the same fault parameters as those used for Figure 8. Thin black lines show the surface projection of 1 m contours of coseismic slip on the subduction interface, bold black lines show the surface traces of prominent fore-arc faults, and black dashed lines show the positions of the trench and 50 km contour to the Wadati-Benioff zone. Field locations described in section 3 are labeled (SC, Salar del Carmen; P, Paposo).

faults in the Antofagasta region could experience either an increase or decrease in Coulomb stress during a strong subduction earthquake, depending on the position of the fault relative to the coseismic slip distribution. Therefore, a subduction zone earthquake has the potential to encourage either normal or reverse faulting, depending on the existing state of stress on a particular upper plate fault. The coseismic near-surface (1 km depth) stress field due to the Antofagasta earthquake (Figure 11) is complicated but provides a mechanism for the apparently contradictory observations of normal and reverse faulting on the Salar del Carmen and Paposo segments of the AFS (section 3), and potentially other fore-arc faults, as they lie within a region that experienced negative $\Delta\sigma_c$ as a result of the earthquake. As the sign convention is defined for this paper, negative $\Delta\sigma_c$ resolved on fore-arc faults discourages normal fault motion or, if the sign of the shear stress change is appropriate, may encourage reverse failure on these structures. It is interesting to note that the narrow zone of negative $\Delta\sigma_c$ mimics the region of positive $\Delta\sigma_c$ of the interseismic model, emphasizing that the short-wavelength patterns of the near-surface stress field need to be considered in each period of the seismic cycle, particularly given the longitudinally restricted distribution of fore-arc crustal faults.

6. Discussion

6.1. Effects of Dislocation Geometry on Surface Stress

[25] Elastic models are limited by unrealistic rheological assumptions. These models do, however, allow for a simple analysis of the subduction zone seismic cycle, providing first-order insight into the processes that drive near-surface deformation. The deformation field predicted by a dislocation model is dependent on the geometry of the applied dislocation. As noted by *Savage* [1983], surface strain in a modeled subduction zone setting is concentrated above the downdip extent of the locked part of the plate boundary (Figure 9). We note that the zone of positive interseismic $\Delta\sigma_c$, analogous to extensional trench-perpendicular strain, in the Coastal Cordillera coincides roughly, but not exactly, with the downdip extent of the modeled plate boundary. Increasing the width of the fully coupled and/or downdip transitional region decreases the magnitude, increases the width, and shifts the position of this anomalous zone (Figure 9). The pattern of surface deformation does not change substantially when a different curvature factor (equation (1)) is used within the transition zones. If slip deficit is applied to a sufficiently wide portion of the plate boundary, the sign of shallow $\Delta\sigma_c$ in the coastal regions changes from positive to zero to negative. However, the width of the coupled zone required to cause this reduction of $\Delta\sigma_c$ to below zero is inconsistent with constraints from seismic and geodetic studies [*Tichelaar and Ruff*, 1991; *Bevis et al.*, 2001; *Klotz et al.*, 2001; *Khazaradze and Klotz*, 2003; *Chlieh et al.*, 2004]. In central and southern Chile (south of 34°S), the width of the coupled zone is greater than in northern Chile due to the shallower dip of the subducting plate [*Khazaradze and Klotz*, 2003]. This greater width of interplate locking would result in an interseismic stress field lacking the positive $\Delta\sigma_c$ anomaly seen in our models of northern Chile, which may serve as an explanation for the pervasive crustal reverse faulting observed there [*Melnick et al.*, 2006].

[26] *Savage* [1983] showed that the zone of extensional trench-normal strain above the lower extent of the subduction thrust (Figure 9) could be eliminated by smoothly tapering the slip deficit from its maximum rate to zero over a finite distance. In our models, we apply a smoothing function within the transition zones in order to minimize abrupt changes in slip deficit magnitude that could lead to stress singularities within the elastic half-space. Despite this constraint, the zone of positive $\Delta\sigma_c$ persists near the surface in coastal regions. Numerous studies correlating the distribution of aftershocks to the $\Delta\sigma_c$ resulting from a strong earthquake show concentrations of aftershocks within the regions of elevated $\Delta\sigma_c$ near the main shock fault plane terminations, suggesting that the stress concentrations near fault tips exert influence on the deformation fields of the material surrounding them [e.g., *King et al.*, 1994; *Toda et al.*, 1998; *Toda and Stein*, 2002; *Kilb et al.*, 2002; *Lin and Stein*, 2004]. Furthermore, the positive $\Delta\sigma_c$ near the coast is

coincident with the region of interseismic uplift, and so the positive $\Delta\sigma_c$ is consistent with the stresses induced along the outer surface of an upward flexed body. *Riquelme et al.* [2003] demonstrated that Neogene uplift of the Coastal Cordillera relative to the Central Depression, just to its east, is accommodated by vertical motion on the Atacama Fault System, providing a link between the regions of uplift and normal faulting.

[27] *Bevis et al.* [2001] and *Khazaradze and Klotz* [2003] interpreted differences between GPS-measured velocities and those modeled using elastic dislocations as representative of permanent strain not predicted by the interplate slip deficit models. In both cases, permanent deformation is inferred to take place in regions of the Andean back arc. Additionally, *Khazaradze and Klotz* [2003] calculate statistically significant east-west extension based on residual GPS velocities, defined as the difference between the actual velocities and those calculated in their preferred model, in the fore arc between 29°S and 34°S, coinciding with N–S striking normal faulting observed between 30°S and 31°S [*Heinze*, 2003]. We suggest that the interseismic stress field is itself capable of shaping the permanent strain exhibited by fore-arc structures, as it is eventually manifested in permanent deformation by driving slip on upper plate faults [e.g., *Pollitz*, 2003; *Allmendinger et al.*, 2005, 2007].

6.2. Spatial Implications

[28] The $\Delta\sigma_c$ map (Figure 8) shows that modeling a change in the extent of interplate locking around the latitude of the Mejillones Peninsula predicts a stress field consistent with distribution of faulting around Antofagasta. Similar correlations between the distribution of interplate coupling and permanent deformation exist elsewhere in the fore arc. Near the city of Iquique, around 20.5°S, the 50 km Wadati-Benioff zone contour line [*Cahill and Isacks*, 1992] and zone of positive $\Delta\sigma_c$ trend offshore, consistent with the distribution of faults. South of Antofagasta, normal faults also project offshore following the trend of the downdip extent of our modeled locked plate boundary (Figure 8a) and coincident zone of positive $\Delta\sigma_c$ (Figure 8b).

[29] The Mejillones Peninsula itself lies entirely within a zone of negative $\Delta\sigma_c$, yet it features several examples of recent normal faulting [*Delouis et al.*, 1998; *González et al.*, 2003; *Allmendinger and González*, 2010]. We suggest several potential reasons for the discrepancy between the deformation fields. The peninsula is a first-order anomaly of northern Chile: it protrudes prominently from the otherwise linear coastline, is located at the same latitude as the Salar de Atacama, which interrupts the linear trend of Andean volcanoes along the arc, and is characterized by a strongly positive gravity anomaly. The peninsula has been recognized as a boundary between earthquake rupture segments on the plate boundary [*Delouis et al.*, 1997]. Earthquakes along the northernmost Chile segment of the margin in 1877 and 2007 are interpreted to have terminated rupture at the peninsula [*Comte and Pardo*, 1991; *Delouis et al.*, 1997; *Loveless et al.*, 2010] and the 1995 Antofagasta earthquake initiated beneath the southern edge of the peninsula and propagated southward [*Delouis et al.*, 1997; *Ihmlé and Ruegg*, 1997; *Sobiesiak*, 2004]. The physical properties that allow the Mejillones Peninsula to serve as a barrier to rupture may affect the nature of interseismic coupling beneath it. Postseismic afterslip following the 1995 earthquake occurs at a rate faster than plate convergence beneath the peninsula [e.g., *Chlieh et al.*, 2004; *Pritchard and Simons*, 2006], suggesting that the plate interface there may not be fully locked [*Pritchard and Simons*, 2006]. A much shallower maximum coupling depth (not considered by our interseismic models) would introduce heterogeneity in the upper plate stress field that may encourage normal faulting observed on the peninsula.

[30] Elevations on the west coast of the Mejillones Peninsula reach nearly 1000 m and lie 75 km from the 7000 m deep trench, resulting in a steep continental slope. *Wang and He* [1999] describe a gravitational trenchward "stretching" force brought about by the presence of fore-arc topography, and the magnitude of this force is positively correlated with the gradient of the continental slope. Bathymetric data reveal numerous slump faults on the continental slope; these and the faults onshore are attributed to gravitational trenchward extension [*von Huene and Ranero*, 2003; *von Huene et al.*, 2004; *Sallarés and Ranero*, 2005]. Subduction erosion processes remove material from the upper plate at the subduction trench, allowing the continental slope to "spread" toward the trench [*von Huene and Ranero*, 2003; *von Huene et al.*, 2004; *Sallarés and Ranero*, 2005]. The consequences of subduction erosion, including subsidence of the continental slope, development of a ~1 km thick "subduction channel" on the plate interface, and incorporation of fore-arc material into arc magma, have thus far been measured on million year timescales [e.g., *von Huene and Ranero*, 2003; *Kay et al.*, 2005], yet the effects on decadal timescales are poorly understood. We consider the extension induced by gravity as a long-term, static effect that is modulated by stress changes related to the seismic cycle.

6.3. Conceptual Models for Coulomb Stress Evolution

[31] *Delouis et al.* [1998] suggest that subduction erosion processes place the fore arc in an extensional tectonic regime and the observed normal faulting occurs due to coseismic enhancement of this extension. *González et al.* [2003] agree, noting that the restriction of faulting to the Mejillones Peninsula and AFS is consistent with the location of maximum coseismic extension accompanying the 1995 Antofagasta earthquake [*Klotz et al.*, 1999]. The models of interseismic deformation presented here complement these results, providing a mechanism for the extensional tectonic regime of *Delouis et al.* [1998], restricted to a narrow longitudinal zone encompassing the Coastal Cordillera. These models of stress change and surface uplift also provide quantification of the suggestion of *González et al.* [2003] that extensional faulting may result from upward flexure driven by plate convergence.

[32] We present three conceptual models for the evolution of the state of stress on upper plate faults in response to the

subduction zone earthquake cycle in Figure 12. All models show the changes in stress on an upper plate fault during 5 interseismic periods separated by 4 roughly periodic interplate earthquakes, the occurrences of which are shown as vertical gray lines. The interseismic stress change is linear with time at the same rate in all seismic cycles. Postseismic deformation is neglected. The coseismic stress change magnitude is different for each earthquake, as it depends on the exact distribution of coseismic slip [e.g., *Loveless and Pritchard*, 2008]. More importantly, the sign of the coseismic stress change can be either positive or negative, based on the location of the upper plate fault with respect to the megathrust rupture zone (e.g., Figure 11).

[33] Figure 12a shows the model of *Delouis et al.* [1998] in which normal faulting is discouraged during the interseismic period. This reflects the orogen-scale pattern of interseismic stress change and neglects our predicted narrow, shallow zone of positive $\Delta\sigma_c$ where faults are concentrated. The elastic rebound effect of strong subduction zone earthquakes induces positive stress change on upper plate faults, encouraging normal failure. Assuming that the coseismic and interseismic stresses do not completely cancel each other, stress on upper plate faults accumulates over several seismic cycles. Eventually, a subduction zone earthquake increases the Coulomb failure stress on the upper plate fault to its critical level for normal faulting, σ_c^n. This slip reduces the magnitude of stress on the fault to a level favoring neither normal nor reverse failure (labeled "A").

[34] Figure 12b shows a modified conceptual model for upper plate fault stress evolution throughout the seismic cycle that incorporates the main results of our stress change modeling. The fault experiences an increase in stress during the interseismic period of the subduction earthquake cycle. Earthquake 1 abruptly increases the stress on the fault and the subsequent interseismic period further pushes the fault toward normal faulting. Due to occurrence on different segments of the subduction zone, earthquake 2 decreases the magnitude of stress on the fault, as does earthquake 3, reducing the likelihood of normal failure. The slip distribution of earthquake 4, however, is such that stress on the fault is increased to σ_c^n. This normal failure of the fault reduces the stress magnitude to the background level A.

[35] Figure 12c can be interpreted as representing the evolution of stress on a fault other than that shown in Figure 12b and addresses the structural observations presented in section 3. In this model, the fault is pushed toward normal failure during the first interseismic period and as a result of earthquake 1. During the subsequent interseismic period, stress again increases gradually, and because of the

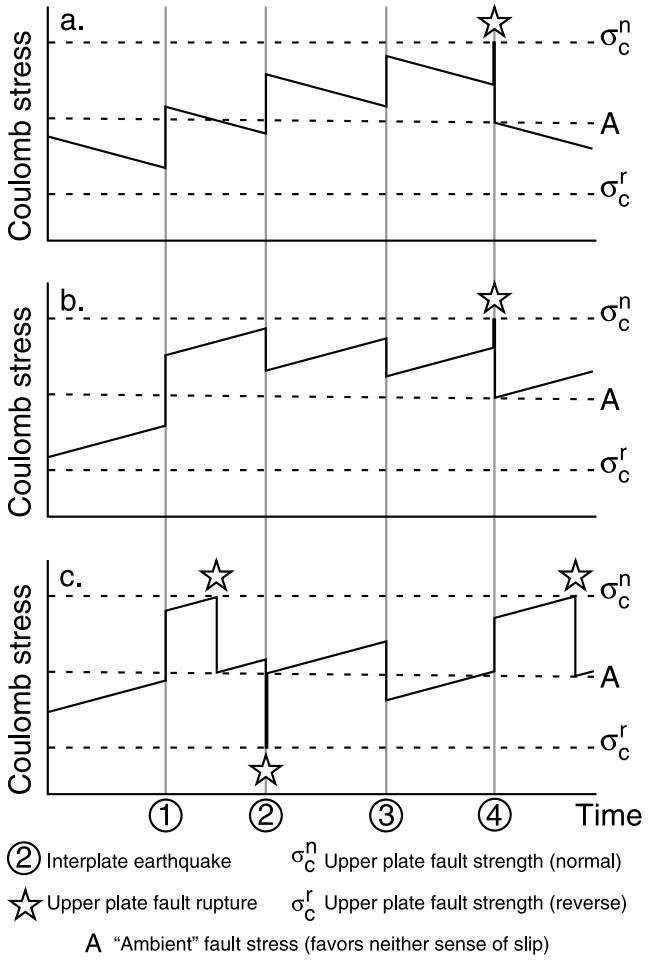

Figure 12. Conceptual models of the state of Coulomb stress (σ_c) on upper plate faults induced by the seismic cycle. Here, positive σ_c refers to the stress encouraging normal failure on the upper plate faults, while negative σ_c favors reverse failure. Gray vertical lines are quasiperiodic and mark the occurrence of major subduction zone earthquakes. Interseismic $\Delta\sigma_c$ is shown as accumulating linearly with time and ignores the effects of postseismic deformation. The parameter σ_c^n refers to the critical value of σ_c at which the fault slips in a normal sense, σ_c^r denotes the value at which the fault slips in a reverse sense, and A represents a background or ambient level of stress favoring neither normal nor reverse failure. (a) Simple model of σ_c evolution presented by *Delouis et al.* [1998]. During the interseismic period, faults are brought further away from normal failure, while strong subduction earthquakes increase σ_c. (b) Revised model of σ_c evolution induced by the seismic cycle, based on the simulations presented in this paper. During the interseismic period, faults are brought closer to normal failure. Depending on the location of a particular upper plate fault relative to the distribution of coseismic slip on the subduction interface, great earthquakes may either increase (1 and 4) or reduce (2 and 3) σ_c. (c) Model illustrating the effect of the existing state of stress on the fault response to the seismic cycle. Because of the state of stress on the fault, different behaviors are possible, including normal fault rupture during the interseismic period of the subduction zone earthquake cycle, and reverse faulting driven by a subduction zone earthquake. See section 6.3 for further discussion.

stress that had previously accumulated on the fault, normal failure occurs in the middle of the interseismic period. This drops the stress on the fault to the background magnitude A, and stress resumes accumulation due to interseismic flexure. Earthquake 2 induces a decrease in stress and, because the state of stress was near its background level due to the recent failure, causes a reduction of the stress on the fault to the level required for reverse faulting, σ_c^r. The act of reverse faulting brings the stress back to the background level, and the interseismic period then gradually increases the level of stress. Earthquakes 3 and 4 cause abrupt changes to the stress state, but it is not until the middle of the interseismic period following earthquake 4 that the conditions on the fault are again appropriate for failure. This model conceptually explains two key phenomena: reverse fault rupture on fore-arc faults, and rupture of faults during the interseismic period of the subduction zone earthquake cycle.

6.4. Mechanical Implications of New Structural Data

[36] The AFS shows a long history of reactivation. *Scheuber and González* [1999] propose that the AFS originated at ~125 Ma, following three stages of deformation within the Jurassic–Early Cretaceous volcanic arc. Therefore, the development of the AFS proper likely involved reactivation of older weaknesses in the crust. We suggest that the damage sustained to the AFS throughout the Mesozoic and Cenozoic plays an important role in dictating its response to the contemporary stress field. Our structural observations indicate that minor amounts of reverse faulting are superimposed on dominantly normal faults. Though the ages of fault slip of any sense are poorly constrained, morphological evidence indicates that both normal and reverse slip has occurred during the Quaternary along various parts of the AFS. At the reverse fault localities on both the Paposo and Salar del Carmen segments, stream incision patterns are used as indicators of reverse faulting, demonstrating that the reverse faulting occurred between the most recent and penultimate episodes of substantial fluvial downcutting. Our suggestion that the seismic cycle is the primary cause of both normal and reverse faulting implies that the two modes of faulting are contemporaneous; the "active" mode is dictated by the mechanical conditions of the fault zone as well as the sense of acting stress field.

[37] The maximum magnitude of near-surface stress change induced by one 100–150 year interseismic period [*Comte and Pardo*, 1991] or one strong subduction earthquake is on the order of 0.5 MPa, about 50 times smaller than the lithostatic stress at even 1 km depth (25 MPa, given a crustal density of 2600 kg/m^3). For such low magnitude stresses to drive fault slip, slip must occur at a very shallow depth, consistent with our reverse faulting observations, and/or the absolute stress within the deforming part of the fault zones themselves must be very low. This in turn implies that the fault zones are very weak, indicating a low coefficient of friction, elevated pore fluid pressure, or a reduced modulus of rigidity within the fault zone as compared to the surrounding rock [e.g., *Fialko et al.*, 2002]. The concept that fore-arc fault zones are weak is consistent with the fact that they have sustained substantial damage by persistent faulting since ~125 Ma. The Coulomb failure stresses σ_c^n and σ_c^r (defined in section 6.3 and Figure 12) are thus likely to be low, allowing the small magnitude $\Delta\sigma_c$ induced by the seismic cycle to drive either reverse or normal faulting. *González et al.* [2006] suggest that at least three discrete episodes of fault slip since 424 ± 151 ka have constructed a suite of alluvial terraces found along the Salar del Carmen segment of the AFS. In the extreme case where only three events have constructed the modern geometry, the mean repeat time is 141 ± 50 ka. Incorporating the fault mechanics and recurrence interval into the model presented in Figure 12c involves reducing the slope of the interseismic $\Delta\sigma_c$ and the magnitude of the coseismic $\Delta\sigma_c$ relative to σ_c^n and σ_c^r. This serves to decrease the frequency of upper plate ruptures, from one rupture every few seismic cycles (i.e., several hundred years), as shown in Figure 12c, to one rupture every thousand seismic cycles (~150 kyr).

7. Conclusions

[38] Our elastic modeling predicts that convergence across the Andean plate boundary interface produces stress within a narrow longitudinal zone that is consistent with the normal faulting on north-south striking structures. The complicated interseismic stress field is mirrored by the coseismic stress field generated by the 1995 Antofagasta earthquake, which shows a narrow zone along the coastline in which reverse faulting is encouraged on the observed faults, providing a mechanism for the opposite senses of slip that we observe along fore-arc fault zones. The elastic rebound model [*Reid*, 1910; *Savage*, 1983] suggests that all interseismic deformation is released by subduction zone earthquakes, but our field observations and modeling results suggest that some seismic cycle stress drives the evolution of permanent structures in the Coastal Cordillera. Seismic hazard analysis for northern Chile therefore requires consideration not only of the major plate boundary earthquake cycle, but also an upper plate fault cycle that may or may not coincide with the interplate seismic pattern; upper plate seismic fault slip may be encouraged exclusively by subduction zone earthquakes, or it could take place during the interseismic period of the subduction cycle. The pervasive damage sustained by the region since the Mesozoic allows low magnitudes of stress to cause permanent strain, and the hyperarid climate of the Atacama Desert preserves evidence of this deformation over long periods of time.

[39] **Acknowledgments.** We thank associate editor Paul Kapp, Michele Cooke, and an anonymous referee for detailed, thoughtful reviews that improved the manuscript. David Pollard and the Stanford Geomechanics Group graciously provided an academic license for Poly3D. We used the open-source meshing program Gmsh [*Geuzaine and Remacle*, 2009] to create the boundary element mesh. Some figures were prepared using the public domain Generic Mapping Tools [*Wessel and Smith*, 1998]. We gratefully acknowledge support from NASA Earth System Science Fellowship grant NNG-04-GQ-94-H (to J.P.L.) and NSF grants EAR-0337496 (to R.W.A.) and EAR-0738507 (to R.W.A. and M.E.P.).

References

Allmendinger, R. W., and G. González (2010), Neogene to Quaternary tectonics of the coastal Cordillera, northern Chile, *Tectonophysics*, doi:10.1016/j.tecto.2009.04.019, in press.

Allmendinger, R. W., R. Smalley Jr., M. Bevis, H. Caprio, and B. Brooks (2005), Bending the Bolivian orocline in real time, *Geology*, *33*(11), 905–908, doi:10.1130/G21779.1.

Allmendinger, R. W., R. Reilinger, and J. Loveless (2007), Strain and rotation rate from GPS in Tibet, Anatolia, and the Altiplano, *Tectonics*, *26*, TC3013, doi:10.1029/2006TC002030.

Arabasz, W. J. (1971), Geological and geophysical studies of the Atacama fault zone, in northern Chile, Ph.D. thesis, Calif. Inst. of Technol., Pasadena.

Armijo, R., and R. Thiele (1990), Active faulting in northern Chile: Ramp stacking and lateral decoupling along a subduction plate boundary?, *Earth Planet. Sci. Lett.*, *98*(1), 40–61, doi:10.1016/0012-821X(90)90087-E.

Beeler, N. M., R. W. Simpson, S. H. Hickman, and D. A. Lockner (2000), Pore fluid pressure, apparent friction, and Coulomb failure, *J. Geophys. Res.*, *105*(B11), 25,533–25,542, doi:10.1029/2000JB900119.

Bevis, M., E. Kendrick, R. Smalley Jr., B. Brooks, R. Allmendinger, and B. Isacks (2001), On the strength of interplate coupling and the rate of back arc convergence in the central Andes: An analysis of the interseismic velocity field, *Geochem. Geophys. Geosyst.*, *2*(11), 1067, doi:10.1029/2001GC000198.

Brooks, B. A., M. Bevis, R. Smalley Jr., E. Kendrick, R. Manceda, E. Lauria, R. Maturana, and M. Araujo (2003), Crustal motion in the southern Andes (26°–36°S): Do the Andes behave like a microplate?, *Geochem. Geophys. Geosyst.*, *4*(10), 1085, doi:10.1029/2003GC000505.

Cahill, T. A., and B. L. Isacks (1992), Seismicity and shape of the subducted Nazca Plate, *J. Geophys. Res.*, *97*(B12), 17,503–17,529, doi:10.1029/92JB00493.

Carrizo, D., G. González, and T. Dunai (2008), Constricción neógena en la cordillera de la costa norte de Chile: Neotectónica y datación de superficies con ^{21}Ne cosmogénico, *Rev. Geol. Chile*, *35*(1), 1–38, doi:10.4067/S0716-02082008000100001.

Chlieh, M., J. B. de Chabalier, J. C. Ruegg, R. Armijo, R. Dmowska, J. Campos, and K. L. Feigl (2004), Crustal deformation and fault slip during the seismic cycle in the North Chile subduction zone, from GPS and InSAR observations, *Geophys. J. Int.*, *158*(2), 695–711, doi:10.1111/j.1365-246X.2004.02326.x.

Comte, D., and M. Pardo (1991), Reappraisal of great historical earthquakes in the northern Chile and southern Peru seismic gaps, *Nat. Hazards*, *4*(1), 23–44, doi:10.1007/BF00126557.

Comte, D., M. Pardo, L. Dorbath, C. Dorbath, H. Haessler, L. Rivera, A. Cisternas, and L. Ponce (1994), Determination of seismogenic interplate contact zone and crustal seismicity around Antofagasta, northern Chile using local data, *Geophys. J. Int.*, *116*, 553–561, doi:10.1111/j.1365-246X.1994.tb03279.x.

Delouis, B., A. Cisternas, L. Dorbath, L. Rivera, and E. Kausel (1996), The Andean subduction zone between 22 and 25°S (northern Chile): Precise geometry and state of stress, *Tectonophysics*, *259*, 81–100, doi:10.1016/0040-1951(95)00065-8.

Delouis, B., et al. (1997), The M_w = 8.0 Antofagasta (Northern Chile) earthquake of 30 July 1995: A precursor to the end of the large 1877 gap, *Bull. Seismol. Soc. Am.*, *87*(2), 427–445.

Delouis, B., H. Philip, L. Dorbath, and A. Cisternas (1998), Recent crustal deformation in the Antofagasta region (northern Chile) and the subduction process, *Geophys. J. Int.*, *132*, 302–338, doi:10.1046/j.1365-246x.1998.00439.x.

Dunai, T. J., G. A. L. González, and J. Juez-Larré (2005), Oligocene-Miocene age of aridity in the Atacama Desert revealed by exposure dating of erosion-sensitive landforms, *Geology*, *33*(4), 321–324, doi:10.1130/G21184.1.

Fialko, Y., D. Sandwell, D. Agnew, M. Simons, P. Shearer, and B. Minster (2002), Deformation on nearby faults induced by the 1999 Hector Mine earthquake, *Science*, *297*(5588), 1858–1862, doi:10.1126/science.1074671.

Flück, P., R. D. Hyndman, and K. Wang (1997), Three-dimensional dislocation model for great earthquakes of the Cascadia subduction zone, *J. Geophys. Res.*, *102*(B9), 20,539–20,550, doi:10.1029/97JB01642.

Geuzaine, C., and J.-F. Remacle (2009), Gmsh: A three-dimensional finite element mesh generator with built-in pre- and post-processing facilities, *Int. J. Numer. Methods Eng.*, *79*(11), 1309–1331, doi:10.1002/nme.2579.

González, G., and D. Carrizo (2003), Segmentación, cinemática y chronología relativa de la deformación tardía de la Falla Salar del Carmen, Sistema de Fallas Atacama, (23°40′S), norte de Chile, *Rev. Geol. Chile*, *30*(2), 223–244, doi:10.4067/S0716-02082003000200005.

González, G., J. Cembrano, D. Carrizo, A. Macci, and H. Schneider (2003), The link between forearc tectonics and Pliocene-Quaternary deformation of the Coastal Cordillera, northern Chile, *J. South Am. Earth Sci.*, *16*, 321–342, doi:10.1016/S0895-9811(03)00100-7.

González, G., T. Dunai, D. Carrizo, and R. Allmendinger (2006), Young displacements on the Atacama Fault System, northern Chile from field observations and cosmogenic ^{21}Ne concentrations, *Tectonics*, *25*, TC3006, doi:10.1029/2005TC001846.

Hampel, A., and R. Hetzel (2008), Slip reversals on active normal faults related to the inflation and deflation of magma chambers: Numerical modeling with application to the Yellowstone-Teton region, *Geophys. Res. Lett.*, *35*, L07301, doi:10.1029/2008GL033226.

Hartley, A. J., and G. Chong (2002), Late Pliocene age for the Atacama Desert: Implications for the desertification of western South America, *Geology*, *30*(1), 43–46, doi:10.1130/0091-7613(2002)030<0043:LPAFTA>2.0.CO;2.

Heinze, B. (2003), Active intraplate faulting in the forearc of north central Chile (30°–31°S): Implications from neotectonic field studies, GPS data, and elastic dislocation modeling, Ph.D. thesis, Freie Univ. Berlin, Berlin, Germany.

Ihmlé, P. F., and J. Ruegg (1997), Source tomography by simulated annealing using broad-band surface waves and geodetic data: Application to the M_w = 8.1 Chile 1995 event, *Geophys. J. Int.*, *131*, 146–158, doi:10.1111/j.1365-246X.1997.tb00601.x.

Kay, S. M., E. Godoy, and A. Kurtz (2005), Episodic arc migration, crustal thickening, subduction erosion, and magmatism in the south-central Andes, *Geol. Soc. Am. Bull.*, *117*(1–2), 67–88, doi:10.1130/B25431.1.

Kelleher, J. A. (1972), Rupture zones of large South American earthquakes and some predictions, *J. Geophys. Res.*, *77*(11), 2087–2103, doi:10.1029/JB077i011p02087.

Kendrick, E., M. Bevis, R. Smalley Jr., and B. Brooks (2001), An integrated crustal velocity field for the central Andes, *Geochem. Geophys. Geosyst.*, *2*(11), 1066, doi:10.1029/2001GC000191.

Khazaradze, G., and J. Klotz (2003), Short- and long-term effects of GPS measured crustal deformation rates along the south central Andes, *J. Geophys. Res.*, *108*(B6), 2289, doi:10.1029/2002JB001879.

Kilb, D., J. Gomberg, and P. Bodin (2002), Aftershock triggering by complete Coulomb stress changes, *J. Geophys. Res.*, *107*(B4), 2060, doi:10.1029/2001JB000202.

King, G. C., R. S. Stein, and J. Lin (1994), Static stress changes and the triggering of earthquakes, *Bull. Seismol. Soc. Am.*, *84*(3), 935–953.

Klotz, J., et al. (1999), GPS-derived deformation of the Central Andes including the 1995 Antofagasta M_w = 8.0 earthquake, *Pure Appl. Geophys.*, *154*, 709–730, doi:10.1007/s000240050249.

Klotz, J., G. Khazaradze, D. Angermann, C. Reigber, R. Perdomo, and O. Cifuentes (2001), Earthquake cycle dominates contemporary crustal deformation in central and southern Andes, *Earth Planet. Sci. Lett.*, *193*(3–4), 437–446, doi:10.1016/S0012-821X(01)00532-5.

Lay, T., and S. Y. Schwartz (2004), "Coupling" semantics and science in earthquake research, Comment, *Eos Trans. AGU*, *85*(36), 339–340, doi:10.1029/2004EO360003.

Lin, J., and R. S. Stein (2004), Stress triggering in thrust and subduction earthquakes and stress interaction between the southern San Andreas and nearby thrust and strike-slip faults, *J. Geophys. Res.*, *109*, B02303, doi:10.1029/2003JB002607.

Loveless, J. P., and M. E. Pritchard (2008), Motion on upper-plate faults during subduction zone earthquakes: Case of the Atacama Fault System, northern Chile, *Geochem. Geophys. Geosyst.*, *9*, Q12017, doi:10.1029/2008GC002155.

Loveless, J. P., G. D. Hoke, R. W. Allmendinger, G. González, B. L. Isacks, and D. A. Carrizo (2005), Pervasive cracking of the northern Chilean Coastal Cordillera: New evidence for forearc extension, *Geology*, *33*(12), 973–976, doi:10.1130/G22004.1.

Loveless, J. P., M. E. Pritchard, and N. Kukowski (2010), Testing mechanisms of subduction zone segmentation and seismogenesis with slip distributions from recent Andean earthquakes, *Tectonophysics*, doi:10.1016/j.tecto.2009.05.008, in press.

Melnick, D., B. Bookhagen, H. P. Echtler, and M. R. Strecker (2006), Coastal deformation and great subduction earthquakes, Isla Santa María, Chile (37°S), *Geol. Soc. Am. Bull.*, *118*(11–12), 1463–1480, doi:10.1130/B25865.1.

Naranjo, J. A. (1987), Interpretación de la actividad cenozoica superior a lo largo de la zona de Falla de Atacama, norte de Chile, *Rev. Geol. Chile*, *31*, 43–55.

Niemeyer, H., G. González, and E. Martinez-de los Ríos (1996), Evolución tectónica cenozoica del margen continental activo de Antofagasta, norte de Chile, *Rev. Geol. Chile*, *23*(2), 165–186.

Okada, Y. (1985), Surface deformation due to shear and tensile faults in a half-space, *Bull. Seismol. Soc. Am.*, *75*(4), 1135–1154.

Okada, Y. (1992), Internal deformation due to shear and tensile faults in a half-space, *Bull. Seismol. Soc. Am.*, *82*(2), 1018–1040.

Oleskevich, D. A., R. D. Hyndman, and K. Wang (1999), The updip and downdip limits to great subduction earthquakes: Thermal and structural models of Cascadia, south Alaska, SW Japan, and Chile, *J. Geophys. Res.*, *104*(B7), 14,965–14,991, doi:10.1029/1999JB900060.

Pacheco, J. F., L. R. Sykes, and C. H. Scholz (1993), Nature of seismic coupling along simple plate boundaries of the subduction type, *J. Geophys. Res.*, *98*, 14,133–14,159, doi:10.1029/93JB00349.

Pollitz, F. F. (2003), The relationship between the instantaneous velocity field and the rate of moment release in the lithosphere, *Geophys. J. Int.*, *153*, 595–608, doi:10.1046/j.1365-246X.2003.01924.x.

Pritchard, M. E., and M. Simons (2006), An aseismic slip pulse in northern Chile and along-strike variations in seismogenic behavior, *J. Geophys. Res.*, *111*, B08405, doi:10.1029/2006JB004258.

Pritchard, M. E., M. Simons, P. A. Rosen, S. Hensley, and F. H. Webb (2002), Co-seismic slip from the 1995 July 30 M_w = 8.1 Antofagasta, Chile earthquake as constrained by InSAR and GPS observa-

tions, *Geophys. J. Int.*, *150*, 362–376, doi:10.1046/j.1365-246X.2002.01661.x.

Pritchard, M. E., C. Ji, and M. Simons (2006), Distribution of slip from 11 $M_w > 6$ earthquakes in the northern Chile subduction zone, *J. Geophys. Res.*, *111*, B10302, doi:10.1029/2005JB004013.

Puskas, C. M., R. B. Smith, C. M. Meertens, and W. L. Chang (2007), Crustal deformation of the Yellowstone-Snake River Plain volcano-tectonic system: Campaign and continuous GPS observations, 1987–2004, *J. Geophys. Res.*, *112*, B03401, doi:10.1029/2006JB004325.

Rech, J. A., J. Quade, and W. S. Hart (2003), Isotopic evidence for the source of Ca and S in soil gypsum, anhydrite and calcite in the Atacama Desert, Chile, *Geochim. Cosmochim. Acta*, *67*(4), 575–586, doi:10.1016/S0016-7037(02)01175-4.

Rech, J. A., B. S. Currie, G. Michalski, and A. M. Cowan (2006), Neogene climate change and uplift in the Atacama Desert, Chile, *Geology*, *34*(9), 761–764, doi:10.1130/G22444.1.

Reid, H. F. (1910), The mechanics of the earthquake, in *The California Earthquake of April 18, 1906*, vol. 2, 192 pp., Carnegie Inst. of Washington, Washington, D. C.

Riquelme, R., J. Martinod, G. Herail, J. Darrozes, and R. Charrier (2003), A geomorphological approach to determining the Neogene to Recent tectonic deformation in the Coastal Cordillera of northern Chile (Atacama), *Tectonophysics*, *361*(3–4), 255–275, doi:10.1016/S0040-1951(02)00649-2.

Ruegg, J., et al. (1996), The M_w = 8.1 Antofagasta (north Chile) earthquake of July 30, 1995: First results from teleseismic and geodetic data, *Geophys. Res. Lett.*, *23*(9), 917–920, doi:10.1029/96GL01026.

Sallarés, V., and C. R. Ranero (2005), Structure and tectonics of the erosional convergent margin off Antofagasta, north Chile (23°30′S), *J. Geophys. Res.*, *110*, B06101, doi:10.1029/2004JB003418.

Savage, J. C. (1983), A dislocation model of strain accumulation and release at a subduction zone, *J. Geophys. Res.*, *88*(B6), 4984–4996, doi:10.1029/JB088iB06p04984.

Scheuber, E., and P. A. M. Andriessen (1990), The kinematic and geodynamic significance of the Atacama fault zone, northern Chile, *J. Struct. Geol.*, *12*(2), 243–257, doi:10.1016/0191-8141(90)90008-M.

Scheuber, E., and G. González (1999), Tectonics of the Jurassic-Early Cretaceous magmatic arc of the North Chilean Coastal Cordillera (22°–26°S): A story of crustal deformation along a convergent plate boundary, *Tectonics*, *18*(5), 895–910, doi:10.1029/1999TC900024.

Sobiesiak, M. M. (2004), Fault plane structure of the 1995 Antofagasta earthquake (Chile) derived from local seismological parameters, Ph.D. thesis, Univ. Potsdam, Potsdam, Germany.

Thomas, A. L. (1993), Poly3D: A three-dimensional, polygonal element, displacement discontinuity boundary element computer program with applications to fractures, faults, and cavities in the Earth's crust, M.S. thesis, Stanford Univ., Stanford, Calif.

Tichelaar, B. W., and L. J. Ruff (1991), Seismic coupling along the Chilean subduction zone, *J. Geophys. Res.*, *96*(B7), 11,997–12,022, doi:10.1029/91JB00200.

Toda, S., and R. S. Stein (2002), Response of the San Andreas fault to the 1983 Coalinga-Nuñez earthquakes: An application of interaction-based probabilities for Parkfield, *J. Geophys. Res.*, *107*(B6), 2126, doi:10.1029/2001JB000172.

Toda, S., R. S. Stein, P. A. Reasenberg, J. H. Dieterich, and A. Yoshida (1998), Stress transferred by the 1995 M_w = 6.9 Kobe, Japan shock: Effect on aftershocks and future earthquake probabilities, *J. Geophys. Res.*, *103*(B10), 24,543–24,565, doi:10.1029/98JB00765.

von Huene, R., and C. R. Ranero (2003), Subduction erosion and basal friction along the sediment-starved convergent margin off Antofagasta, Chile, *J. Geophys. Res.*, *108*(B2), 2079, doi:10.1029/2001JB001569.

von Huene, R., W. Weinrebe, and F. Heeren (1999), Subduction erosion along the North Chile margin, *J. Geodyn.*, *27*, 345–358, doi:10.1016/S0264-3707(98)00002-7.

von Huene, R., C. R. Ranero, and P. Vannucchi (2004), Generic model of subduction erosion, *Geology*, *32*(10), 913–916, doi:10.1130/G20563.1.

Wang, K., and T. Dixon (2004a), "Coupling" semantics and science in earthquake research, *Eos Trans. AGU*, *85*(18), 180–181, doi:10.1029/2004EO180005.

Wang, K., and T. Dixon (2004b), "Coupling" semantics and science in earthquake research, Reply, *Eos Trans. AGU*, *85*(36), 340, doi:10.1029/2004EO360004.

Wang, K., and J. He (1999), Mechanics of low-stress fore arcs: Nankai and Cascadia, *J. Geophys. Res.*, *104*(B7), 15,191–15,205, doi:10.1029/1999JB900103.

Wang, K., R. Wells, S. Mazzotti, R. D. Hyndman, and T. Sagiya (2003), A revised dislocation model of interseismic deformation of the Cascadia subduction zone, *J. Geophys. Res.*, *108*(B1), 2026, doi:10.1029/2001JB001227.

Wessel, P., and W. H. F. Smith (1998), New, improved version of Generic Mapping Tools, *Eos Trans. AGU*, *79*, 579, doi:10.1029/98EO00426.

R. W. Allmendinger and M. E. Pritchard, Department of Earth and Atmospheric Sciences, Cornell University, Snee Hall, Ithaca, NY 14853, USA.

G. González, Departmento de Ciencias Geológicas, Universidad Católica del Norte, Casilla 1280, Antofagasta, Chile.

J. P. Loveless, Department of Earth and Planetary Sciences, Harvard University, 20 Oxford St., Cambridge, MA 02138, USA. (loveless@eps.harvard.edu)